

Gram-scale cryogenic calorimeters for rare-event searches

R. Strauss,^{1,*} J. Rothe,¹ G. Angloher,¹ A. Bento,² A. Gütlein,³ D. Hauff,¹ H. Kluck,³ M. Mancuso,¹ L. Oberauer,⁴ F. Petricca,¹ F. Pröbst,¹ J. Schieck,³ S. Schönert,⁴ W. Seidel,^{1,†} and L. Stodolsky¹

¹Max-Planck-Institut für Physik, D-80805 München, Germany

²CIUC, Departamento de Física, Universidade de Coimbra, P3004 516 Coimbra, Portugal

³Institut für Hochenergiephysik der Österreichischen Akademie der Wissenschaften, A-1050 Wien, Austria, and Atominstytut, Vienna University of Technology, A-1020 Wien, Austria

⁴Physik-Department, Technische Universität München, D-85748 Garching, Germany

(Dated: May 28, 2022)

The energy threshold of a cryogenic calorimeter can be lowered by reducing its size. This is of importance since the resulting increase in signal rate enables new approaches in rare-event searches, including the detection of MeV mass dark matter and coherent scattering of reactor or solar neutrinos. A scaling law for energy threshold vs. detector size is given. We analyze the possibility of lowering the threshold of a gram-scale cryogenic calorimeter to the few eV regime. A prototype 0.5 g Al₂O₃ device achieved an energy threshold of (19.7 ± 0.1) eV, the lowest value reported for a macroscopic calorimeter.

Cryogenic calorimetry [1] is based on the idea that the temperature rise in a target after an energy deposition ΔE is given by

$$\Delta T = \frac{\Delta E}{C} \quad (1)$$

where C is the heat capacity of the object. A small C , which can be achieved in crystalline materials at \sim mK temperatures, leads to a large temperature jump and so to a high sensitivity to small energies. State-of-the-art cryogenic detectors with a mass of 300 g can reach energy thresholds down to \sim 300 eV [2].

A further reduction of the threshold is of great interest since for many important processes, such as the coherent neutrinos nucleus scattering (CNNS) or the scattering of the hypothetical dark matter (DM) particles, the count rate increases greatly as the threshold of a detector is lowered. In Fig. 1 we show the count rate for some processes as a function of energy, together with background rates at different setups. One observes that a threshold in the 10 eV regime can allow the count rates to rise significantly above background levels. CNNS at a nuclear reactor is in reach and the technology offers unique possibilities for the detection of MeV DM and solar neutrinos.

Since macroscopic amounts of target material are necessary to obtain reasonable count rates for such weak interaction processes, microscopic calorimeters with target masses below milligrams are impractical for rare-event searches. Here we describe how it is possible to achieve a suitably low threshold with a small but macroscopic calorimeter, and present the results of a 0.5 g prototype.

A straight forward application of Eq. 1 would seem to suggest that an improved response for small energies is to be achieved by simply reducing C by lowering the temperature or using smaller devices [1].

However, there are some subtleties in applying Eq. 1. For example it may apply not to the whole device in question, but to some sensitive subsystem. This explains why

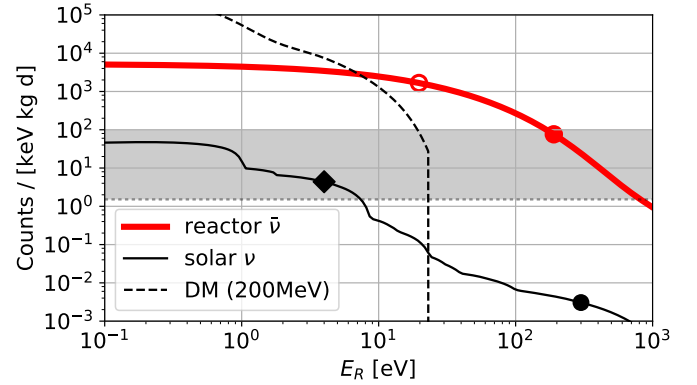


FIG. 1. Nuclear-recoil spectra on CaWO₄ for CNNS of anti-neutrinos from a 4 GW nuclear reactor at a distance of 40 m, for 200 MeV mass DM ($\sigma = 1$ pb), and for CNNS of solar neutrinos. The grey area indicates a range of measured background levels for well-shielded surface sites and at an underground location (dotted line) [3]. Dots indicate previous cryogenic detector technology [2, 4], the performance of the detector presented here is depicted as a circle (surface operation) and a diamond (underground operation).

we obtain results with macroscopic devices, on the order of grams in mass, which one would have thought only possible with very small or microscopic systems. Below we report an energy threshold of \sim 20 eV – which is in the order of atomic binding energies – for a 0.5 g device operated under unshielded conditions.

To understand this surprising result, we consider the operation of the detectors similar to those used in CRESST for direct dark matter search [2, 5]. These detectors operate out of thermal equilibrium after an energy deposition. The signal originates from the initial “ballistic” non-thermal phonons of the particle event occurring in the “absorber” crystal. The deposited energy is measured using a superconducting transition-edge-sensor (TES). This is explained at length in Ref. [6], and we use

the terminology and notation of this reference. In particular we deal with detectors operating in the “calorimetric mode” (section 3.3.1 in [6]), where the film thermalizes slowly with respect to the signal duration and so integrates the energy of the incoming non-thermal phonons. This results in a temperature rise in the thermometer film given by

$$\Delta T_{\text{film}} = \epsilon \Delta E / C_e \quad (2)$$

where ϵ is the fraction of the deposited energy ΔE thermalized in the film, and C_e is the heat capacity of the electrons in the film.

Since $\epsilon \Delta E$ is the energy absorbed in the film, Eq. 2 amounts to Eq. 1, but applied to the electrons of the superconducting film. Their temperature rise and thus our readout signal is given by a pulse whose magnitude originates in a microscopic system, although the detector itself is macroscopic.

This discussion suggests that by suitable design and tuning, various transient effects could be used to detect very small energies. A fundamental limitation only arises through the fact that for very small C a body coupled to a heat bath has large irreducible temperature fluctuations $(\Delta T/T)^2 = 1/C$ [7], where we use $k_B = 1$. This is not a significant limitation for the detectors we consider ($C \sim 10^8$ for the W film used here), but it does set a limit on an indefinite reduction of C .

A simple scaling law enables us to extrapolate results with previous CRESST detectors to smaller sizes. This is possible on the basis of Eq. 2. We are interested in the threshold energy E_{th} , which is inversely proportional to the temperature rise ΔT_{film} for a given energy deposition.

We consider cubes corresponding to the CRESST main absorbers, for which there is considerable data. To anticipate, we arrive at the following approximate scaling law for the threshold energy vs. the mass M of the detector.

$$E_{th} = (\text{const.}) \times M^{2/3}, \quad (3)$$

The proportionality constant will depend on the material, shape and other factors but not on the size of the crystal.

Eq. 3 results from Eq. 2 as follows. The appearance of ϵ , representing the fraction of the original non-thermal phonons thermalizing in the film shows that the main effect entering in Eq. 2 is the competition between the thermalization in the superconducting film and the thermalization on the surfaces of the crystal. We expect that ϵ is small due to the great difference in the respective surface areas. We have then that ϵ is simply given by the ratio of thermalization rates which we call κA for the film and crystal respectively, so that $\epsilon = \frac{\kappa_{\text{film}} A_{\text{film}}}{\kappa_{\text{crystal}} A_{\text{crystal}}}$, where the κ refer to material and other parameters and the A to the surface areas. Inserting in Eq. 2 and keeping only factors related to size, one obtains

$$\epsilon \frac{\Delta E}{C_e} = \frac{\kappa_{\text{film}} A_{\text{film}}}{\kappa_{\text{crystal}} A_{\text{crystal}}} \frac{\Delta E}{C_e} \propto \frac{1}{A_{\text{crystal}}}, \quad (4)$$

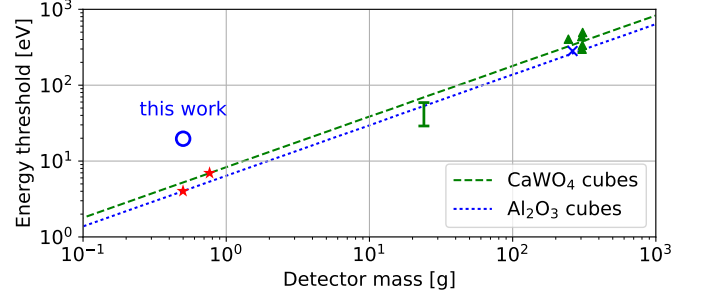


FIG. 2. The scaling law for CaWO_4 and Al_2O_3 cubes fitted to results of cryogenic CaWO_4 (triangles) and Al_2O_3 (cross) detectors [2, 8, 9]. The lines show the $M^{2/3}$ behavior according to Eq. 3. The expected values for the prototype described here under low-background conditions is shown by the red stars. There is agreement with the expected performance of 24 g CaWO_4 detectors (green error bar) [4]. The result presented here is shown by a blue circle.

where we have left out all factors that do not depend on the crystal size in the last step. A_{film} has cancelled because $C_e \propto V_{\text{film}} = A_{\text{film}} h$, and the films all have about the same thickness h . Eq. 4 shows that the main effect in reducing the size of the crystals is to reduce their surface area and so increase the signal correspondingly. For a cube one has $A_{\text{crystal}} \propto d^2$ and $M \propto d^3$ where d is the edge length. Since the threshold varies inversely as the pulse height or ΔT_{film} , we obtain Eq. 3.

Fig. 2 shows the scaling law for CaWO_4 (dashed line) and Al_2O_3 (dotted line) calorimeters versus mass operated in the CRESST low-background setup, here referred to as benchmark setup. The offset between the green and blue lines is due to the different density and sound-speed of the materials and due to material-dependent transmission properties of phonons into the superconducting film (total factor ~ 0.86). The model is fitted to the results of CaWO_4 detectors with $M = 250 - 300$ g (triangles) used in CRESST-II [2, 8] and a Al_2O_3 cube of $M = 262$ g (cross) used in CRESST-I [9]. The scaling law nicely matches the performance of 24 g CaWO_4 detectors for CRESST-III as expected from a prototype measurement (error bar) [4]. Red stars indicate the projected performance of $(5 \times 5 \times 5)$ mm³ CaWO_4 and Al_2O_3 calorimeters at the benchmark setup. Below we discuss the result of the first version of a 0.5 g Al_2O_3 detector operated in a surface test setup (blue circle).

For the first test of a gram-scale calorimeter, a Al_2O_3 cube of $(5 \times 5 \times 5)$ mm³ with a mass of ~ 0.5 g was used. All surfaces are optically polished. The cube was equipped with a W thin film TES similar to those used for CRESST light detectors [10]. The TES design was adjusted for operation in the “calorimetric mode” [6] on the cubic crystal.

The data presented here were acquired in a cryostat at the Max-Planck-Institut (MPI) for Physics in Mu-

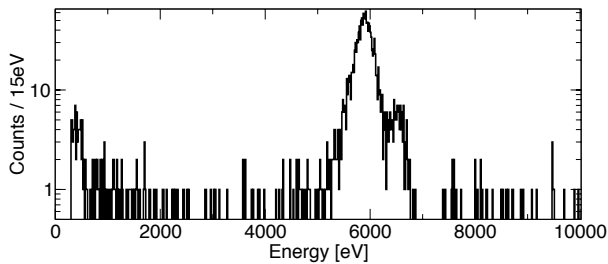


FIG. 3. Final energy spectrum up to 10 keV acquired with the prototype Al_2O_3 detector in presence of a ^{55}Fe calibration source (the region below 300 eV is blinded until the DM results are published).

nich, Germany. The setup at surface-level had no shielding against environmental radio-activity or cosmogenic backgrounds. The crystal is placed on three Al_2O_3 spheres with a diameter of 1 mm resting on a copper plate and providing point-like contacts. From the top, a bronze clamp (with a central Al_2O_3 sphere) presses on the cube. The electrical and thermal connections are realized by Al and Au wire bonds (diameter $25\text{ }\mu\text{m}$), respectively. The cryostat reached a base temperature of 6 mK and the mixing chamber was stabilized during the measurement at 11 mK. The W TES on the Al_2O_3 crystal showed a normal-to-superconducting transition at 22 mK. The readout current (detector bias) was fixed at $1.0\text{ }\mu\text{A}$, yielding a maximum signal-to-noise ratio. Commercial SQUID magnetometers and a state-of-the-art data acquisition system was used [5].

A ^{55}Fe X-ray calibration source with an activity of 0.6 Bq was installed about 2 cm from the Al_2O_3 cube. The data is from a total measuring time of 5.3 h corresponding to an exposure of 0.11 g-days. The total particle pulse rate was 0.36 Hz of which $\gtrsim 40\%$ was from the X-ray lines of the ^{55}Fe calibration source.

The energy of an event is inferred from its pulse height. The pulses were fitted by a template pulse extracted from an energy region where the pulse response is completely linear, in this case around $\sim 0.32\text{ V}$, which corresponds to an energy of about 0.47 keV. The detector response becomes increasingly non-linear at about 3 keV. To reconstruct the energy of large, saturated pulses the method of a truncated template fit was used [5]. The pulse shape is fitted in the linear region up to the truncation limit, which here is chosen at 0.4 V. Fig. 3 shows the final energy spectrum up to 10 keV after stability and data quality cuts (see e.g. [2, 8]). The dominant K_α line ($E_{lit} = 5.898\text{ keV}$) is found to have a pulse height of $(3.925 \pm 0.003)\text{ V}$ and is used for the calibration of the pulse spectrum. The energy of the K_β line on the shoulder is then reproduced at an energy of $E_{K_\beta} = (6.485 \pm 0.017)\text{ keV}$, which is in good agreement with the literature value of 6.490 keV. This demonstrates the linearity of the detector response up to this energy

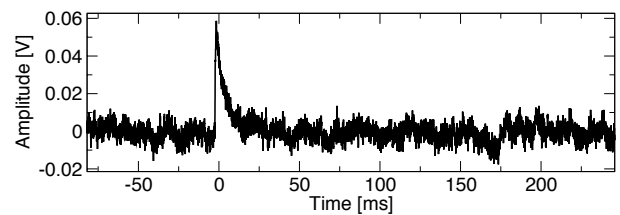


FIG. 4. A randomly selected pulse with an energy of $\sim 100\text{ eV}$. The clarity of this rather low energy event shows the effectiveness of the small (0.5 g) cryogenic calorimeter.

range. Furthermore, the quality of the template fit [5] shows no significant energy dependence up to these energies. Above $\sim 15\text{ keV}$, strong saturation effects prevent a precise pulse-height reconstruction. The energy resolution of the X-ray lines is $\sigma_{\text{Fe}} = (0.147 \pm 0.005)\text{ keV}$ which is about 40 times larger than the baseline resolution at zero energy, as determined from the variance of the baseline (see below). This strong energy dependence of the detector resolution was observed previously for cryogenic Al_2O_3 detectors [11].

The measurement shows a constant background rate of $\sim 1.2 \cdot 10^5\text{ counts/[kg keV day]}$ (7-10 keV) above the calibration peaks, see Fig. 3. This background index is not unexpected due to the lack of any shielding against ambient and cosmogenic backgrounds. At lower energies ($\lesssim 1\text{ keV}$) the event rate significantly rises towards threshold. Auger electrons from the ^{55}Fe source and surface-contamination induced backgrounds are the most plausible explanation for this increase. Fig. 4 shows a randomly chosen particle pulse with an energy of 100 eV.

For the pulse height evaluation at low energies, the optimum filter method is used (see e.g. [12, 13]). The optimum filter maximizes the signal-to-noise for a known signal, in our case the template pulse, in the presence of stochastic noise with a known power spectrum. To build the filter transfer function, the Fourier transform of the template pulse and the noise power spectrum are required. Here, the latter is derived from ~ 400 randomly chosen baseline samples. In the selection of the baseline samples the same quality cuts were applied as for the pulse samples. In the frequency domain, the optimum filter weights the spectral components according to their signal-to-noise ratio. Usually the filter is applied in frequency space to minimize the computing time and is then transformed back to the time domain. The result is normalized so that it reproduces the unfiltered pulse height at the pulse's maximum.

The baseline energy resolution after filtering is found to be $\sigma_b = (3.74 \pm 0.21)\text{ eV}$. This compares to a value of $(6.89 \pm 0.32)\text{ eV}$ without filtering, showing a clear improvement. This effect reduces the energy threshold accordingly which can be exploited when using a data acquisition system that continuously streams the detector

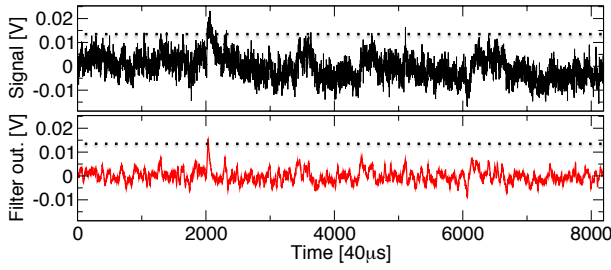


FIG. 5. Demonstration of the optimum trigger. Upper plot: A 19.7 eV standard pulse is superimposed on a randomly chosen noise sample (onset at sample 2000). Lower plot: Output of the optimum filter applied to the sample. The pulse is clearly triggered while noise contributions are suppressed sufficiently below threshold which is set at a pulse height of 13.0 mV (see text).

output (here operated in parallel to the standard data acquisition). The functionality of such a software trigger based on the optimum filter is illustrated in Fig. 5. A small artificial pulse is superimposed on a randomly selected baseline sample, drawn in the upper frame. The lower frame shows the optimum filter output. The artificially added pulse clearly is seen above a given threshold (dotted line), while the random noise, which has a different pulse shape, is suppressed.

In the following we discuss how the energy threshold and the trigger efficiency can be determined in a direct way. Generally speaking, the threshold on the output of the optimum filter has to be chosen so as to be sensitive to the smallest possible energy depositions, while at the same time suppressing noise triggers sufficiently. Fig. 6 (black histogram, right axis) shows the filter output of a set of pure noise samples. The bulk of the noise samples have a reconstructed energy between 10 and 15 eV, which suggests setting the trigger threshold just above this value. We choose a trigger threshold of 13.0 mV and validate this choice by a study of the trigger efficiency as a function of energy. Onto the set of baseline samples, template pulses of various discrete pulse heights (from about 1 to $10 \cdot \sigma_b$) are added. The energy dependent trigger efficiency is the fraction of the filtered artificial pulse samples which fall above the threshold. Fig. 6 (left axis) shows the results of this procedure for the discrete pulse heights (red crosses). The resulting curve can be nicely fitted by the function $p_{trig}(E) = 0.5 \cdot (1 + \text{erf}[(E - E_{th})/(\sqrt{2}\sigma_{th})])$, where erf is the Gaussian error function [8]. The validity of the threshold choice manifests itself as a vanishing trigger efficiency at low energies, corresponding to negligible noise triggers. Furthermore, the width of the error function is $\sigma_{th} = (3.83 \pm 0.15) \text{ eV}$ which is in good agreement with the baseline noise of $\sigma_b = (3.74 \pm 0.21) \text{ eV}$, demonstrating that the resolution of the detector at these energies is dominated by the baseline noise. The energy threshold

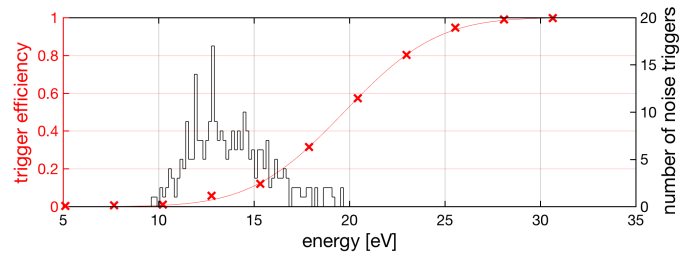


FIG. 6. Determination of the trigger threshold. Randomly chosen noise samples are superimposed with template pulses of different discrete energies (red crosses). The optimum trigger is applied to these samples yielding the energy-dependent trigger efficiency (left y-axis). The data is fitted by an error-function, giving an energy threshold of $E_{th} = (19.7 \pm 0.1) \text{ eV}$ for 50% efficiency. The width $\sigma_{th} = (3.82 \pm 0.15) \text{ eV}$ is in agreement with the variance of the baseline noise. The reconstructed energy of pure noise samples after filtering is shown in a histogram (black, right y-axis).

(by definition at 50% trigger efficiency) is found to be $E_{th} = (19.7 \pm 0.1) \text{ eV}$, which corresponds to $5.27\sigma_b$. In a setup with optimized noise conditions, the threshold can presumably be lowered to $4.5\text{--}5\sigma_b$, a typical value reached in low-background underground environments [8].

The prototype detector shows the lowest energy threshold reported for macroscopic calorimeters, an improvement by one order of magnitude with respect to previous results [4]. Since the device is a calorimeter it should be stressed that its operation does not have the quenching factor problems that arise when dealing with ionization or scintillation detectors. Thus it has the same response for a given energy deposit, regardless of the interacting particle type and can approach energies below the fundamental nuclear-recoil reach of ionization detectors (e.g. 40 eV for Si and Ge [14]). The threshold, shown as a blue circle in Fig. 2, is somewhat higher than predicted by the scaling law, indicated by the red stars. However, this is expected to improve in a low-noise, low background environment.

The threshold is determined by comparing the measured noise with the amplitude of template pulses calibrated with events induced by the ^{55}Fe source. Thus the main assumption in arriving at our very low threshold is in the linear extrapolation of the pulse height-energy relation to low energies. Our threshold lies in a new energy range, never explored with this type of detector. Nevertheless, even these energies corresponds to the creation of very many of the 1 meV non-thermal phonons involved in the detection mechanism [6]. For energy depositions around or below 10 eV there is the possibility of different nuclear recoil mechanisms as one approaches lattice dislocation energies. It could be interesting for rare event searches to attempt a direct calibration at lowest energies, as with recoils from nuclear isomeric transitions or electron capture.

Due to the smallness of the calorimeters presented here, the technology permits new experiments in three aspects: 1) ultra-low energy thresholds down to the 10 eV-regime, 2) encapsulation of the small calorimeters by cryogenic veto detectors and 3) ability to operate the detectors above-ground in a high-rate environment. These features enable interesting possibilities involving the exploitation of the enhancement of the cross section by coherent scattering [15].

In two accompanying papers we discuss the application of such a detector to the search of sub-GeV dark matter and solar neutrinos [16], which should be possible with present crystal background levels, and present details of a setup for laboratory detection of CNNS at a nuclear reactor with a few weeks running time [17]. With this technology, real-time monitoring of nuclear reactor cores for non-proliferation and accident prevention is in reach. The prototype run described here can be used to set a new limit on the spin-independent dark matter particle-nucleon cross section for masses below 500 MeV/c² [16].

[†] Deceased 19 February 2017

- [1] Leo Stodolsky. *Phys. Today*, 44N8:24–32, 1991.
- [2] G. Angloher et al. *Eur. Phys. J.*, C76(1):25, 2016.
- [3] R. Strauss et al. *JCAP*, 1506(06):030, 2015.
- [4] R. Strauss et al. *Nucl. Instrum. Meth.*, A845:414–417, 2017.
- [5] G. Angloher et al. *Eur. Phys. J.*, C72:1971, 2012.
- [6] F. Pröbst et al. *J. Low Temp. Phys.*, 100(1-2):69–104, 1995.
- [7] S. H. Moseley et al. *J. Appl. Phys.*, 56(5):1257–1262, 1984.
- [8] G. Angloher et al. *Eur. Phys. J.*, C74(12):3184, 2014.
- [9] O. Meier et al. *Nucl. Instrum. Meth.*, A444:350–352, 2000.
- [10] G. Angloher et al. *Astropart. Phys.*, 31:270–276, 2009.
- [11] M. Sisti et al. *Nucl. Instrum. Meth.*, A466:499–508, 2001.
- [12] E. Gatti and P. F. Manfredi. *Riv. Nuovo Cim.*, 9N1: 1–146, 1986.
- [13] G. Piperno, S. Pirro, and M. Vignati. *JINST*, 6:P10005, 2011.
- [14] R. Agnese et al. *Phys. Rev. D*, 95:082002, 2017.
- [15] A. Drukier and L. Stodolsky. *Phys. Rev. D*, 30:2295–2309, 1984.
- [16] R. Strauss et al. *to be published*, 2017.
- [17] R. Strauss et al. *arXiv e-print*, 2017.

* Corresponding author: strauss@mpp.mpg.de